Journal of Modern Technology and Engineering
Vol.10, No.3, 2025, pp.213-223
https://doi.org/10.62476/jmte.103213

PERFORMANCE EVALUATION OF PID AND FUZZY LOGIC CONTROL STRATEGIES UNDER CHARGE-DISCHARGE CYCLES IN A SIMSCAPE-BASED THERMAL-ELECTRICAL BATTERY SYSTEM

Rahim Mammadzada*

Department of Instrumentation Engineering, Azerbaijan State Oil and Industry University, Baku, Azerbaijan

Abstract. This paper presents a structured Simscape-based workflow for comparing proportional-integral-derivative (PID) and fuzzy logic controller (FLC) strategies in regulating battery temperature during continuous charge and discharge cycles. Under repeated cycling, nonlinear effects such as varying internal resistance, heat generation, and state of charge changes become more pronounced, often leading to unstable temperature growth and reduced efficiency. Temperature regulation is therefore essential to prevent degradation, ensure safety, and extend battery lifespan. In this study, a single lithium-ion cell is modeled in both electrical and thermal domains, linking input current control directly to temperature feedback. PID and FLC are applied to manage this current, maintaining operation within safe thermal limits. The results show differences in dynamic behavior and control effort between the two methods, with the FLC reducing temperature overshoot while introducing mild undershoot at a stable temperature of $44.73°C$, and reducing settling time from roughly 4500 steps for PID to about 500 steps. Additionally, the FLC improves the root mean square error of temperature regulation from about $5.99°C$ for PID to around $4.35°C$ for FLC. The proposed workflow provides a clear and practical framework for studying temperature-dependent control strategies in thermal electrical systems.

Keywords: Fuzzy Logic Control, Temperature Regulation, Battery Thermal Modeling, MATLAB, Simscape Electrical, Charge–Discharge Dynamics.

AMS Subject Classification: 93C42, 93C15, 81T80.

Corresponding author: Rahim Mammadzada, Department of Instrumentation Engineering, Azerbaijan State Oil and Industry University, Baku, Azerbaijan, e-mail: *rahim.mammadzada02@gmail.com*

Received: 23 October 2025; Revised: 30 November 2025; Accepted: 7 December 2025;
Published: 22 December 2025.

1 Introduction

During continuous charge and discharge operation, batteries experience fluctuations that directly influence their performance, efficiency, and lifespan (Yusubov & Bekirova, 2023). Maintaining stable thermal conditions is essential for ensuring reliability, as overheating accelerates degradation while poor regulation reduces capacity and overall energy output (Sun et al., 2023). The interaction between thermal and electrical effects makes accurate modeling and effective temperature control an important part of battery management (Naguib et al., 2023).

To help address this challenge, MATLAB's Simscape Electrical library provides a dedicated battery block that captures the coupled thermal–electrical behavior of cells. It allows users to simulate how current flow, heat generation, and temperature feedback interact during operation. By linking physical parameters with control algorithms, Simscape offers a unified environment for studying and optimizing battery performance under realistic conditions (Mammadzada, 2025b).

This paper presents a structured Simscape-based workflow for evaluating PID and FLC strategies under the identical charge–discharge conditions in thermal–electrical battery systems.

2 Objective

The study examines current-based temperature regulation using a controlled Simscape environment and compares the behavior of PID and FLC during repeated charge and discharge cycles. A single-cell model is used to keep the focus on control behavior rather than pack-level effects, and the controller settings are defined in a fully reproducible form.

A key contribution of this work is its emphasis on reproducibility, which is often difficult to achieve in application-oriented battery control studies. Many papers rely on lookup tables measured from real cells to maximize controller performance, but these measurements capture the unique characteristics of each battery. This makes it hard for other researchers to obtain matching controller responses or repeat the analysis under identical conditions.

In contrast, the workflow presented here adopts an ideal baseline for both the battery model and the controller settings, ensuring that the entire simulation can be reproduced without relying on cell-specific measurements. By clearly outlining how each parameter is defined, the study provides a structured foundation that others can extend into more detailed models or use to evaluate different control strategies under identical conditions. This addresses an underexplored gap in the literature by offering practical guidance for constructing repeatable simulation frameworks for temperature-regulating controllers in coupled thermal and electrical systems.

3 Materials and Methods

In Figure 1, the complete Simulink model of the temperature control system is shown. The system includes subsystems for the plant, which represent the battery, the error calculation block, the controller, a pulse-width modulation (PWM) to current conversion block, and a charge or discharge mode selector. This configuration allows the controller to regulate current flow based on the temperature feedback.

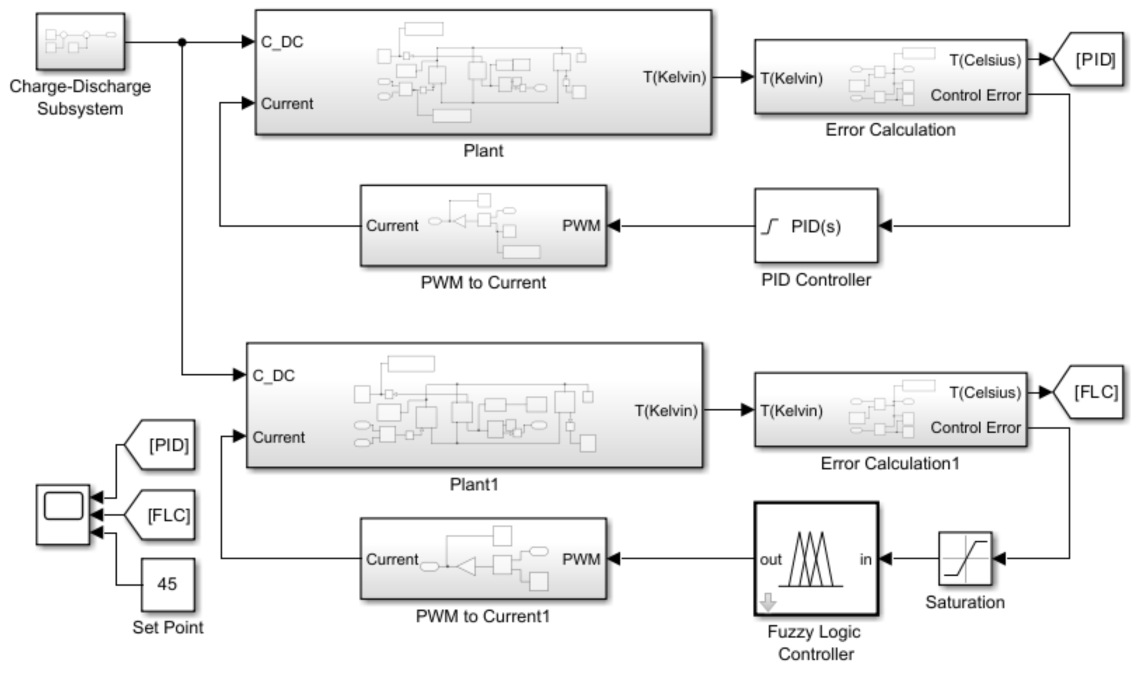

Figure 1: Thermal–Electrical Control System Overview

The thermal behavior of a single battery can be represented by the general heat balance equation, which relates heat generation, accumulation, and dissipation to describe temperature variation over time:

$$C\frac{dT}{dt} = Q_{\text{in}} - Q_{\text{out}} \tag{1}$$

Where C is the thermal capacitance, T is the component temperature, Q_{in} is the heat input from generation or losses, and Q_{out} is the heat dissipated to the environment. These parameters define the thermal response of the battery under varying load conditions. Simscape provides a convenient framework for modeling this interaction by directly linking the electrical domain, where heat is generated, with the thermal domain, where it is dissipated (Mammadzada, 2025a).

The battery subsystem, combining both electrical and thermal domains using Simscape Electrical components, is presented in Figure 2. The electrical side includes a controlled current source driven by the PWM to the current block, while the thermal side includes a thermal mass and a convection block that represent the heat exchange with the surrounding environment. A thermal sensor measures the temperature of the cell and sends this value to the control error calculation subsystem.

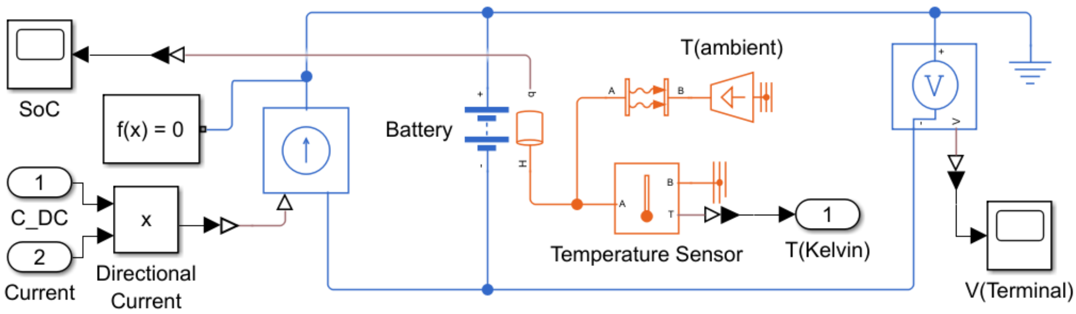

Figure 2: Battery Subsystem with Electrical and Thermal Components

The Simscape Electrical battery block simplifies the modeling of a single cell by combining both electrical and thermal characteristics into a single, parameterized component. It allows users to define key parameters such as nominal voltage, internal resistance, and cell capacity, while also accounting for temperature-dependent effects through a linked thermal port. This enables the automatic computation of heat generation during charge and discharge cycles, which can be coupled with thermal elements such as convection and thermal mass (Mammadzada, 2025c). Consequently, realistic temperature variations and performance responses can be simulated without explicitly formulating the underlying electro-thermal equations.

The parameters used to configure the battery block are listed in Table 1. They correspond to a typical 18650-type lithium-ion cell and are sufficient for demonstrating how the thermal–electrical battery model can be set up for controller performance evaluation.

Table 1: Primary Parameters of the Battery Block

Parameter	Symbol	Value	Unit
Nominal Vorlage	V_{nom}	3.2	V
Internal Resistance	R_{in}	0.035	Ohm
Measurement Temperature	T_m	25	$Celsius$
Thermal Mass	C	81	J/K
Initial Temperature	T_{Init}	30	$Celsius$
Initial Charge	Q_{Init}	6	Ah

By default, the battery block in Simscape Electrical assumes an infinite charge capacity, meaning the cell can theoretically store and release energy without limit. However, for realistic simulations, this assumption must be replaced with a finite-charge model that reflects the actual cell capacity. The parameters used for this configuration are listed in Table 2, which defines how the battery's voltage relates to its remaining charge.

In particular, voltage V_1 represents the open-circuit voltage when the available charge is AH_1, and vice versa. The charge AH_1 corresponds to the remaining ampere-hours when the no-load voltage equals V_1. Together, these values describe how the terminal voltage gradually decreases as the battery discharges, allowing the model to represent the nonlinear relationship between charge and voltage observed in practical cells. In addition, it is important to account for how electrical properties vary with temperature.

Table 2: Finite Charge Configuration Parameters

Parameter	Symbol	Value	Unit
Cell Capacity	Q	6	Ah
Voltage V1 (When Charge is AH1)	V_{Ah1}	3	V
Charge AH1 (When no-load Voltage is V1)	Q_{AH1}	3	Ah

Since no active cooling components are included in this setup, heat dissipation occurs solely through natural convection. The Convection block shown in Figure 2 models this process and requires input parameters surface area and convection coefficients, summarized in Table 3. These values define how effectively the battery can release heat to the surrounding air, influencing temperature rise during continuous charge–discharge cycles.

Table 3: Convection Modeling Parameters

Parameter	Symbol	Value	Unit
Convection Area	A_{conv}	0.007339	V
Heat Transfer Coefficient	h_{nat}	5	$W/(K \times m^2)$
Ambient Temperature	T_{amb}	30	$Celsius$

To determine the total surface area required for convection, the battery's geometric dimensions must be considered. Assuming a cylindrical cell, the overall convection area A_{conv} is obtained by summing the areas of the top circular cap A_{cap} and the curved side surface A_{side}. The corresponding equations for each component were derived separately, ensuring accurate thermal representation.

$$A_{conv} = A_{cap} + A_{side} = \pi r_{bat}^2 + 2\pi r_{bat} h_{bat} \tag{2}$$

The final computed geometric values used in the simulation are presented in Table 4, which consolidates the battery size parameters applied in all subsequent thermal–electrical analyses.

Table 4: Battery Geometry and Surface Area Parameters

Parameter	Symbol	Value	Unit
Battery Height	h_{bat}	0.065	m
Battery Radius	r_{bat}	0.016	m
Battery Cap Area	A_{cap}	0.000804	m^2
Battery Side Area	A_{side}	0.006535	m^2

In addition to geometric and physical properties, the Simscape Electrical battery block incorporates dynamic electrical parameters that influence how the terminal voltage reacts to changing current demands. As listed in Table 5, the time constant and polarization resistance form an RC branch in the equivalent circuit that produces a temporary voltage shift and governs how quickly the voltage settles after a current step. The selected values, a time constant of 30 sec and a polarization resistance of 0.1 ohm, smooth rapid transitions and prevent the terminal voltage from collapsing instantly, which ensures physically meaningful behavior when the state of charge becomes low or when the current direction changes.

Table 5: One time constant time dynamics

Parameter	Symbol	Value	Unit
First polarization resistance	R_{pol1}	0.1	*Ohm*
First time constant	T_{const1}	30	*Sec*

The Battery block's parameters at the second measurement temperature, $45°C$, are presented in Table 6, showing how internal resistance changes with both temperature and voltage. This temperature-dependent behavior becomes accessible only after activating the thermal port, which is disabled by default. Enabling this feature allows the model to reflect heat generation and its influence on electrical performance under dynamic operating conditions.

Table 6: Battery Block Parameters at 45 Celsius Measurement Temperature

Parameter	Symbol	Value	Unit
Nominal Voltage	$V_{nom(45)}$	3.2	*V*
Internal Resistance	$R_{int(45)}$	0.032	*Ohm*
Voltage V1	$V_{1(45)}$	3.1	*V*
First polarization resistance	$R_{pol1(45)}$	0.08	*Ohm*
First time constant	$T_{const1(45)}$	30	*Sec*

Although not intended for precise cell identification, these parameters are sufficient for demonstration purposes and provide a stable basis for comparing the performance of both controllers within the developed model. After describing the battery block and its properties, it is also important to clarify the role of each subsystems that enable closed-loop operation before proceeding to the controller setup.

The error calculation process is illustrated in Figure 3. The measured temperature is converted from kelvin to Celsius and then subtracted from the setpoint to obtain the control error. The set point temperature is defined as $45°C$, which is a commonly accepted safe operating temperature where most batteries maintain optimal performance and stability. This error signal is then passed to the proportional-integral-derivative and the fuzzy logic controller.

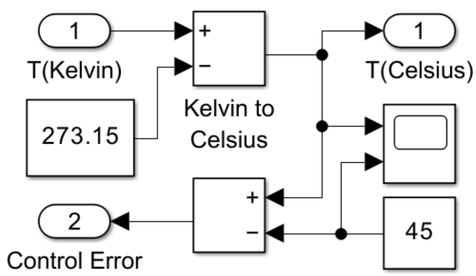

Figure 3: Control Error Calculation Subsystem

The step signal used to represent the charge–discharge cycles applied to the battery model is shown in Figure 4. The signal consists of three distinct segments: it begins with a discharge cycle that continues until step 3600, after which the magnitude switches to -1 to initiate the charging cycle. At step 7200, the signal returns to +1, resuming discharging until step 10800. Then it switches to -1 again until step 14400, followed by a final return to +1 that continues until step 18000. This simple waveform provides a practical and effective way to emulate continuous cycling without adding unnecessary complexity to the controller design. By inverting the current direction through these step changes, the battery block automatically interprets and responds to each transition, allowing realistic charge and discharge behavior to be simulated.

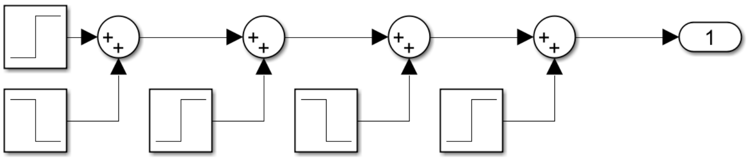

Figure 4: Charge–Discharge Mode Selection Subsystem

The PWM-to-current conversion subsystem is shown in Figure 5. The controller output is first inverted by subtracting one from it, since the control goal is to reduce the input current as the temperature rises. This approach also keeps the signal within the common 0 to 1 PWM range, which simplifies implementation and tuning. Using this positive range avoids issues during PID auto-tuning, where negative control signals can complicate linearization. The resulting normalized signal is then multiplied by a gain block that defines the maximum current flow rate, generating a smooth and realistic current command for the battery model.

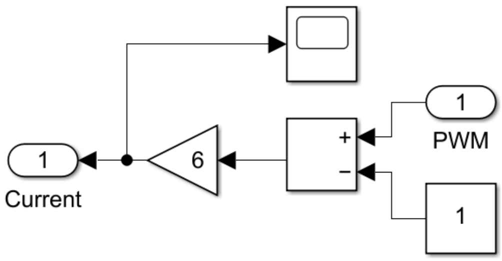

Figure 5: PWM-to-Current Conversion Subsystem

4 Solution Approach

After the thermal electrical model is fully established, the next step is to configure the controllers. The proportional-integral-derivative (PID) controller is set to output saturation of $[0, 1]$, and auto-tuned using the built-in PID Tuner. The resulting gains are around $K_p = 0.0228$ for proportional, $K_i = 2.3717$ for integral, and $K_d = -1.5955$ for derivative branches, and a filter coefficient of $N = 0.0019$ serves as baseline values for the simulation and can be fine-tuned as needed for temperature regulation.

The fuzzy logic controller (FLC) operates as a first-order Sugeno system. Its input universe spans [-1, 1], a range chosen so that control action begins once the temperature exceeds $44°C$ and reaches full strength at $46°C$ and above. Three triangular membership functions shape this input space, labeled *Negative* [-1, -1, -0.16], *Zero* [-0.83, 0, 0.83], and *Positive* [0.16, 1, 1]. The output uses three discrete levels: *Low*, 0, *Medium*, 0.75, and *High*, 1, representing the amount of current reduction applied for temperature control. Here, the rule base maps *Negative* to *Low*, *Zero* to *Medium*, and *Positive* to *High*. These naming conventions follow common practice in the literature and are sufficient for the purposes of this study (Belman-Flores et al., 2022).

The key temperature trends of both controllers across all charge-discharge cycles are summarized in Figure 6. The FLC reaches its steady state early, stabilizing near 44.73°C by step 500 and maintaining a consistent response afterward. The PID controller shows a more dynamic pattern, including an overshoot of about 59.20°C at step 1185, followed later by an undershoot down to about 44.45°C at step 5750. After these two large deviations, the PID response settles, with only small fluctuations for the remainder of the simulation.

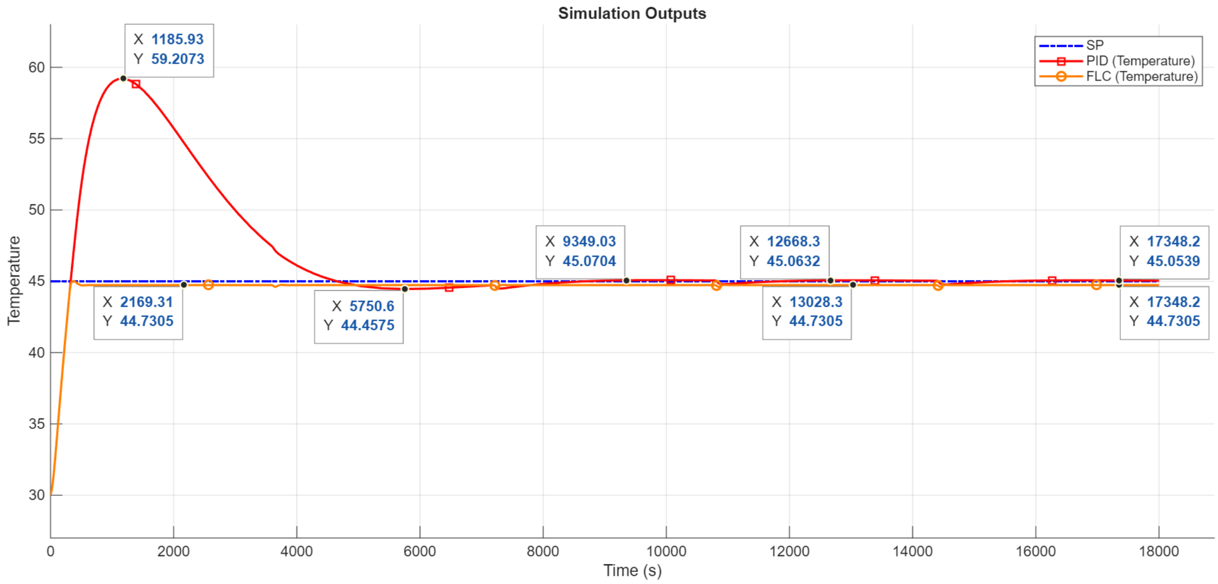

Figure 6: Temperature Response Comparison of PID and Fuzzy Logic Controllers

Building on the trends in Figure 6, the quantitative evaluation of controller performance is summarized in Table 7. Root Mean Square Error (RMSE) represents the overall deviation from the setpoint, capturing both magnitude and frequency of errors. Mean Absolute Error (MAE) indicates the average absolute deviation, providing a simpler measure of typical error. Maximum Deviation (Max Diff) identifies the single largest deviation observed during the simulation. Starting from the 30°C initial condition, the PID exhibits an RMSE of 5.99°C, an MAE of 3.39°C, and a maximum deviation of 15°C, reflecting the overshoot and undershoot observed earlier. Overshoot metrics further quantify stability: Mean Exceed is the average amount by which the temperature rises above the setpoint, Maximum Exceed (Max Exceed) is the worst-case overshoot, and Violations counts the number of distinct excursions above the setpoint. The PID has a mean exceed of 3.76°C, a max exceed of 14.21°C, and four violations, whereas the FLC maintains closer adherence to the setpoint with an RMSE of 4.35°C, an MAE of 1.68°C, the same max deviation of 15°C, a mean exceed of 0.01°C, a max exceed of 0.02°C, and only a single violation. Together, these values confirm that the FLC achieves tighter control with fewer excursions, while the PID experiences larger but temporary deviations before settling.

Table 7: One time constant time dynamics

Controller	RMSE	MAE	Max Diff	Mean Exceed	Max Exceed	Violations
PID	5.9919°C	3.3940 °C	15 °C	3.7594 °C	14.2073 °C	4
FLC	4.3506 °C	1.6780 °C	15 °C	0.0102 °C	0.0188 °C	1

In addition to temperature change, it is also important to understand how the actions of both controllers affected other essential parameters such as current flow, state of charge, terminal voltage, and pulse-width modulation (PWM) signals. For this, simulation results were gathered with the "To Workspace" block, and every fifth step of the output arrays was noted in Table 8.

Table 8: Summary of Simulation Results for FLC and PID Controllers

	PID					**FLC**				
Step	Temp	Current	SoC	V_{term}	PWM	Temp	Current	SoC	V_{term}	PWM
0	30.00	-6.00	21600	2.99	0.00	30.00	-6.00	21600	2.99	0.00
0	30.00	-6.00	21599	2.99	0.00	30.00	-6.00	21599	2.99	0.00
23	30.46	-6.00	21462	2.69	0.00	30.46	-6.00	21462	2.69	0.00
59	31.80	-6.00	21248	2.51	0.00	31.80	-6.00	21248	2.51	0.00
111	34.42	-6.00	20935	2.45	0.00	34.42	-6.00	20935	2.45	0.00
212	39.63	-6.00	20327	2.47	0.00	39.63	-6.00	20327	2.47	0.00
312	44.35	-6.00	19727	2.51	0.00	44.33	-4.90	19730	2.55	0.18
335	45.36	-6.00	19589	2.51	0.00	44.88	-1.50	19666	2.81	0.75
374	47.04	-6.00	19356	2.52	0.00	45.02	-1.50	19608	2.96	0.75
413	48.66	-5.96	19120	2.54	0.01	44.93	-1.50	19549	3.01	0.75
477	51.00	-5.62	18755	2.58	0.06	44.74	-2.11	19442	2.98	0.65
576	53.86	-5.14	18222	2.65	0.14	44.73	-2.22	19218	2.93	0.63
754	57.08	-4.44	17370	2.75	0.26	44.73	-2.20	18828	2.94	0.63
1023	59.02	-3.62	16291	2.84	0.40	44.73	-2.19	18237	2.93	0.63
1517	58.34	-2.64	14764	2.93	0.56	44.73	-2.19	17153	2.93	0.63
2169	54.69	-2.00	13279	2.97	0.67	44.73	-2.19	15723	2.91	0.63
2887	50.54	-1.78	11943	2.95	0.70	44.73	-2.19	14148	2.90	0.63
3600	47.44	1.81	10671	3.03	0.70	44.73	2.19	12584	3.02	0.63
3610	47.39	1.82	10689	3.11	0.70	44.71	2.37	12607	3.13	0.61
3657	47.11	1.84	10775	3.27	0.69	44.62	2.96	12739	3.39	0.51
3713	46.89	1.85	10879	3.31	0.69	44.72	2.25	12885	3.40	0.62
3817	46.58	1.87	11072	3.32	0.69	44.73	2.18	13108	3.38	0.64
4053	45.99	1.92	11518	3.33	0.68	44.73	2.19	13625	3.39	0.63
5031	44.66	2.09	13480	3.37	0.65	44.73	2.19	15771	3.41	0.63
6831	44.64	2.23	17397	3.43	0.63	44.73	2.19	19720	3.44	0.63
7202	44.72	-2.23	18215	3.26	0.63	44.73	-2.21	20525	3.28	0.63
7221	44.66	-2.24	18174	3.11	0.63	44.67	-2.63	20480	3.10	0.56
7272	44.51	-2.26	18057	2.96	0.62	44.64	-2.79	20331	2.91	0.54
7334	44.50	-2.27	17918	2.93	0.62	44.74	-2.14	20184	2.94	0.64
7463	44.56	-2.27	17626	2.92	0.62	44.73	-2.21	19906	2.94	0.63
7802	44.73	-2.27	16856	2.92	0.62	44.73	-2.20	19161	2.94	0.63
9349	45.07	-2.23	13380	2.89	0.63	44.73	-2.19	15767	2.92	0.63
10800	45.06	-2.22	10157	2.84	0.63	44.73	-2.19	12584	2.88	0.63
10807	45.04	2.22	10172	3.05	0.63	44.72	2.29	12599	3.09	0.62
10842	44.89	2.23	10250	3.25	0.63	44.61	2.98	12693	3.34	0.50
10896	44.80	2.25	10371	3.33	0.63	44.69	2.45	12844	3.41	0.59
10965	44.80	2.25	10526	3.35	0.62	44.74	2.11	12995	3.38	0.65
11133	44.85	2.25	10906	3.35	0.63	44.73	2.20	13364	3.38	0.63
11948	45.01	2.24	12735	3.38	0.63	44.73	2.19	15151	3.40	0.63
13748	45.05	2.22	16739	3.42	0.63	44.73	2.19	19100	3.43	0.63
14402	45.03	-2.22	18178	3.26	0.63	44.73	-2.21	20525	3.28	0.63
14421	44.96	-2.22	18137	3.11	0.63	44.66	-2.64	20480	3.10	0.56
14473	44.80	-2.24	18021	2.96	0.63	44.64	-2.78	20331	2.91	0.54
14534	44.78	-2.25	17884	2.93	0.63	44.74	-2.14	20184	2.94	0.64
14663	44.81	-2.25	17592	2.92	0.62	44.73	-2.21	19904	2.94	0.63
15020	44.91	-2.25	16790	2.92	0.63	44.73	-2.20	19121	2.94	0.63
16628	45.06	-2.22	13198	2.89	0.63	44.73	-2.19	15593	2.91	0.63
18000	45.04	-2.22	10155	2.84	0.63	44.73	-2.19	12583	2.88	0.63

The PWM behavior in Figure 7 highlights how these controllers respond as temperature changes through the charge and discharge cycles. The FLC reacts immediately with a sharp rise to about 0.75 PWM to limit early temperature rise, while the PID controller adjusts more slowly, and eventually reaches its own peak of about 0.7. As the system settles, both controllers converge toward a steady value near 0.63 PWM, but they do so with noticeably different styles. The FLC produces brief corrective spikes at each cycle transition that momentarily dip to about 0.5, showing rapid, targeted adjustments whenever conditions shift. In contrast, the PID response smooths out after its early activity and follows a more uniform path with minimal variation. All numerical values supporting these observations are summarized in Table 8.

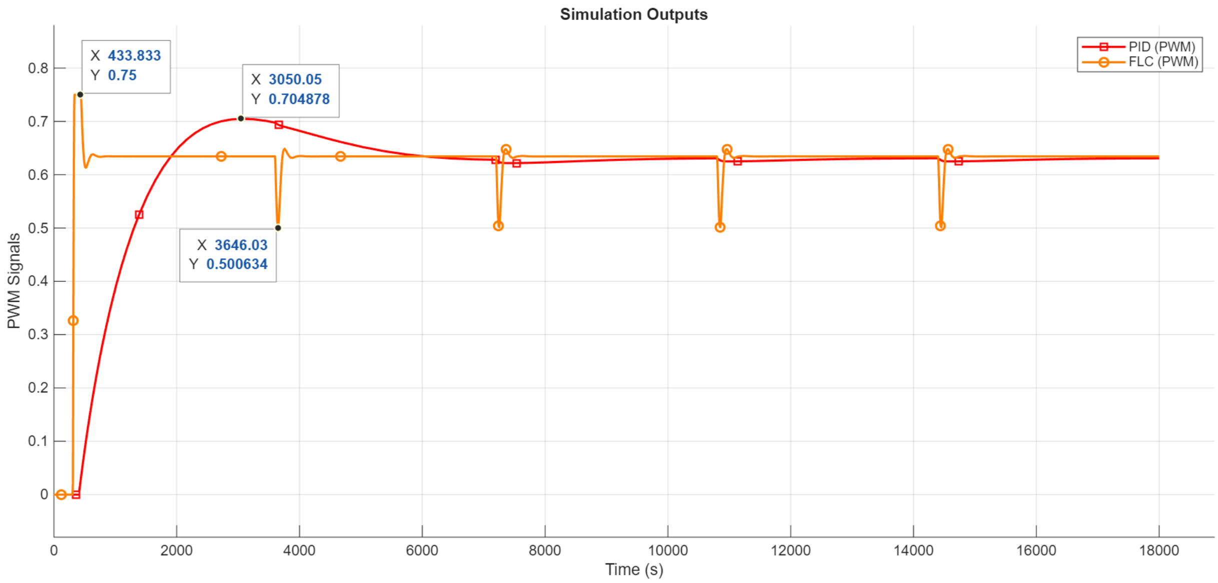

Figure 7: PWM Output Comparison for PID and Fuzzy Logic Controllers

For better clarity on the charge and discharge behavior, Figure 8 presents the resulting current curves, with all numerical values listed in Table 8. The subsystem in Figure 4 enables the mapping of the zero to one PWM range into both charging and discharging currents, allowing the model to produce the full zero to six and zero to minus six ampere range needed for cycling.

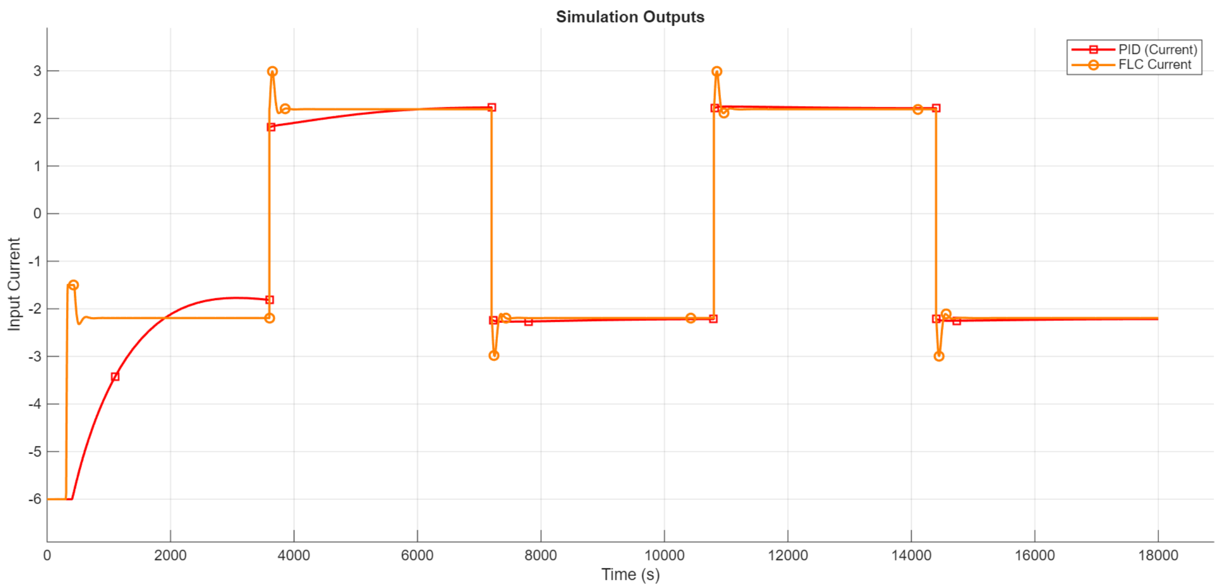

Figure 8: Input Current Profiles for PID and Fuzzy Logic Controllers

The state-of-charge curves in Figure 9 give a clear view of how both controllers handle energy over the full sequence of charge and discharge phases. Because the FLC draws less current during key transitions, its state of charge (SoC) remains consistently higher, reaching peaks of around 20,500 coulombs and descending to about 12,600 coulombs at the end of discharge, with smooth rises at each mode change. The PID controller follows the same overall pattern but shows lower peaks of about 18,200 coulombs and deeper drops to 10,200 coulombs, reflecting its stronger corrective behavior from earlier stages. These differences repeat across all cycles, and the exact SoC values behind these trends are summarized in Table 8.

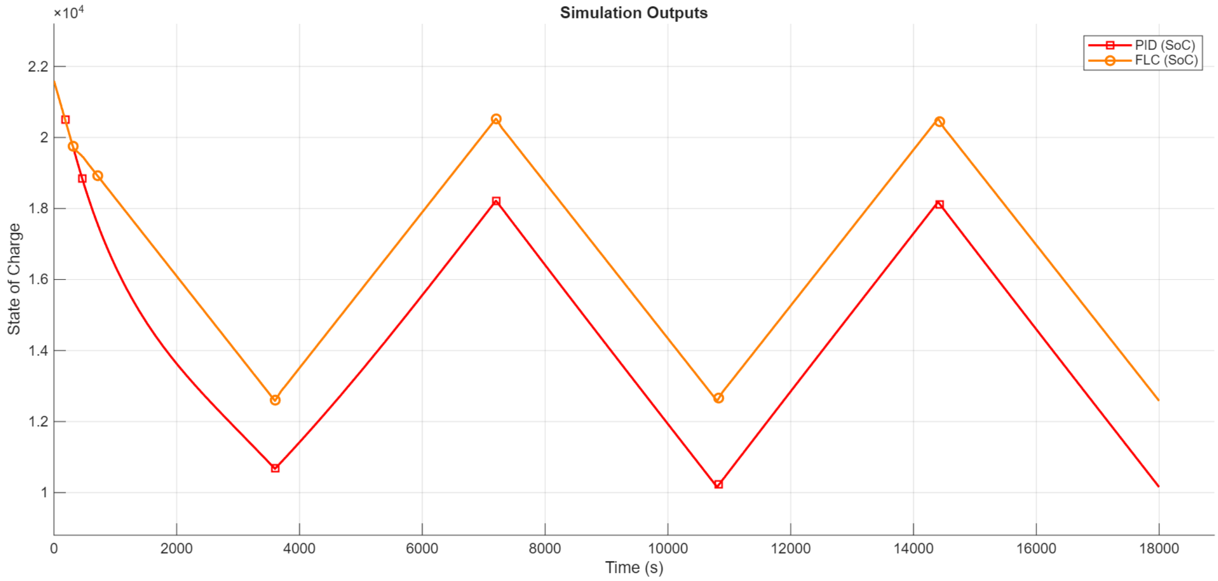

Figure 9: State-of-Charge Comparison Between Controllers

The terminal voltage in Figure 10 follows the charge and discharge cycles from the Figure 4 subsystem, where current magnitude drives voltage changes. During charging, the voltage rises as the battery accepts current, and during discharging, it falls under load. The FLC keeps a smoother, more predictable voltage, matching its steady current and temperature behavior, while the PID shows sharper rises and dips. Table 8 shows all of the terminal voltage values.

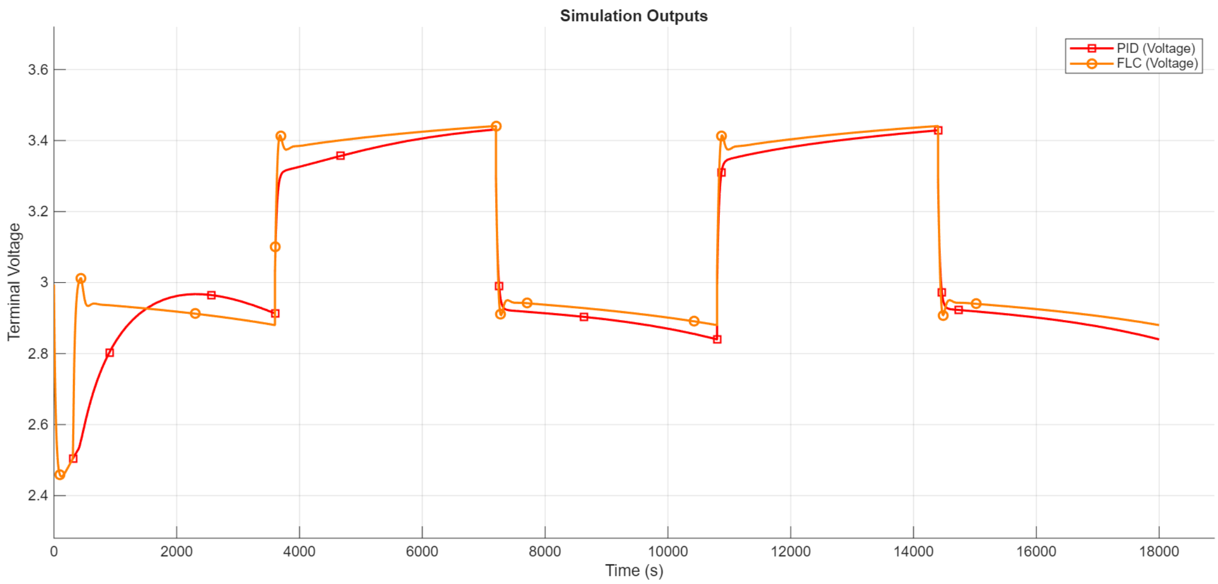

Figure 10: Terminal Voltage Comparison for PID and Fuzzy Logic Controllers

5 Conclusion

This study demonstrates the effectiveness of using the Simscape Electrical battery block for modeling coupled thermal–electrical behavior. The block simplifies realistic battery simulations by integrating electrical and thermal characteristics, allowing inclusion of parameters such as internal resistance, capacity, and temperature-dependent effects without manually deriving complex equations. Its modular nature enables straightforward experimentation with control strategies, providing both educational and research value, and allowing reproducibility for testing different control approaches or varying system parameters.

The comparison between proportional-integral-derivative (PID) and fuzzy logic controller (FLC) highlights clear differences in handling continuous charge and discharge cycles. PID exhibits larger overshoots and undershoots, requires roughly 4500 steps to stabilize, and produces a root mean square error (RMSE) of $5.99°C$, a mean absolute error (MAE) of $3.39°C$, a mean exceedance of $3.76°C$, and 4 violations of thermal limits. In contrast, the FLC nearly eliminates overshoot, limits undershoot to a constant temperature of $44.73°C$, stabilizes in about 500 steps, and improves RMSE to $4.35°C$, MAE to $1.68°C$, with a mean exceedance of $0.01°C$ and only 1 violation. These results demonstrate that PID struggles to manage dynamic thermal-electrical interactions, while FLC provides faster, smoother regulation with lower steady-state deviations.

Beyond controller performance, the study emphasizes the importance of understanding battery dynamics, including state of charge, internal resistance, heat generation, and terminal voltage interactions, which directly affect thermal stability and charge recovery. By investigating these interactions, engineers and researchers gain a practical framework for evaluating control strategies, highlighting the value of Simscape Electrical as a reproducible and flexible tool for designing advanced battery management systems and educational experiments without relying on less transparent application-level simulations.

References

Belman-Flores, J. M., Rodríguez-Valderrama, D. A., Ledesma, S., García-Pabón, J. J., Hernández, D., & Pardo-Cely, D. M. (2022). A review on applications of fuzzy logic control for refrigeration systems. *Applied Sciences*, *12*(3), 1302. https://doi.org/10.3390/app12031302

Naguib, M., Rathore, A., Emery, N., Ghasemi, S., & Ahmed, R. (2023). Robust Electro-Thermal Modeling of Lithium-Ion Batteries for Electrified Vehicles Applications. *Energies*, *16*(16), 5887. https://doi.org/10.3390/en16165887

Sun, T., Wang, L., Ren, D., Shi, Z., Chen, J., Zheng, Y., ... & Ouyang, M. (2023). Thermal runaway characteristics and modeling of $LiFePO_4$ power battery for electric vehicles. *Automotive Innovation*, *6*(3), 414–424. https://doi.org/10.1007/s42154-023-00226-3

Yusubov, E. & Bekirova, L. (2023). The optimized power flow control system for the photovoltaic DC microgrid. *E3S Web of Conferences*, *404*, 03001. https://doi.org/10.1051/e3sconf/202340403001

Mammadzada, R.R. (2025a). Application of fuzzy logic to thermal control using component separation modeling approach, 21. https://www.elibrary.ru/item.asp?id=82947792&pff=1

Mammadzada, R.R. (2025b). Using Simscape to Model a Temperature Control System with Fuzzy Logic for Educational Purposes. https://libeldoc.bsuir.by/handle/123456789/61784

Mammadzada, R. (2025c). A Systematic Approach to Thermal System Modeling with Examples Using First Principles. https://macosep.cyber.az/2025/papers/05.05.html